


MULTIFIDELITY KOLMOGOROV-ARNOLD NETWORKS

A PREPRINT

 **Amanda A. Howard**

Pacific Northwest National Laboratory
Richland, WA 99354
amanda.howard@pnnl.gov

 **Bruno Jacob**

Pacific Northwest National Laboratory
Richland, WA 99354
bruno.jacob@pnnl.gov

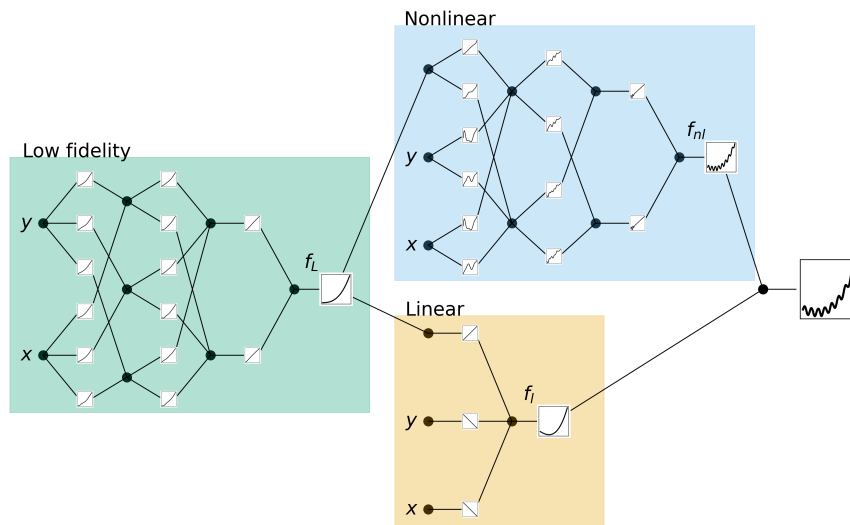
 **Panos Stinis**

Pacific Northwest National Laboratory
Richland, WA 99354
panagiotis.stinis@pnnl.gov

ABSTRACT

We develop a method for multifidelity Kolmogorov-Arnold networks (KANs), which use a low-fidelity model along with a small amount of high-fidelity data to train a model for the high-fidelity data accurately. Multifidelity KANs (MFKANs) reduce the amount of expensive high-fidelity data needed to accurately train a KAN by exploiting the correlations between the low- and high-fidelity data to give accurate and robust predictions in the absence of a large high-fidelity dataset. In addition, we show that multifidelity KANs can be used to increase the accuracy of physics-informed KANs (PIKANs), without the use of training data.

Keywords Kolmogorov-Arnold networks · Multifidelity · Physics-informed neural networks



Graphical abstract: Multifidelity KANs accurately learn from low-fidelity and high-fidelity data simultaneously.

1 Introduction

In recent years, scientific machine learning (SciML) has emerged as a paradigm for modeling physical systems [1, 2, 3]. Typically using the theory of multilayer perceptrons (MLPs), SciML has shown great success in modeling a wide range of applications, however, data-informed training struggles when high-quality data is not available.

Kolmogorov-Arnold networks (KANs) have recently been developed as an alternative to MLPs [4, 5]. KANs use the Kolmogorov-Arnold Theorem as inspiration and can offer advantages over MLPs in some cases, such as for discovering interpretable models. However, KANs have been shown to struggle to reach the accuracy of MLPs, particularly without modifications [6, 7, 8, 9]. In the short time since the publication of [4], many variations of KANs have been developed, including physics-informed KANs (PIKANs)[9], KAN-informed neural networks (KINNs)[10], temporal KANs [11], wavelet KANs [12], graph KANs [13, 14, 15], Chebyshev KANs (cKANs) [16], convolutional KANs [17], ReLU-KANs [18], Higher-order-ReLU-KANs (HRKANs) [19], fractional KANs [20], finite basis KANs [21], deep operator KANs [22], and others. KANs have been applied to fluid dynamics [23, 24], time-series analysis [25], satellite image classification [26], abnormality detection [27], and computer vision [28, 29], among other applications [30].

Multifidelity machine learning uses two or more datasets to train a network more accurately than using either dataset alone [31]. The most common framework is bi-fidelity training with two datasets, denoted by the low-fidelity and high-fidelity datasets. For scientific applications, low-fidelity data is often data generated by a lower-order model or on a coarser mesh. In this way, the low-fidelity data is less expensive to generate, so it is possible to sample a large low-fidelity dataset. However, it is less accurate. The high-fidelity dataset is a small dataset of highly accurate data. The goal of multifidelity training is to train simultaneously with low- and high-fidelity data. Multifidelity machine learning is an increasingly important research field due to the cost of generating and storing highly accurate training data [31, 32, 33]. Several approaches for multifidelity training have been developed, including transfer learning [34, 35, 36, 37, 38, 39, 40, 41, 42], intermediate approaches [43, 44], and composite multifidelity neural networks [45]. Composite multifidelity neural networks have been particularly successful, and have been extended to a large number of variations, including PINNs [45, 46], continual learning [47], deep operator networks [48, 49, 50], Bayesian neural networks [51], and a large number of applications [52, 53], *e.g.*, aerodynamics [54, 55], material properties [56], rotor dynamics [57], and rheology [58, 59, 60, 61].

While KANs have been widely applied, training KANs still relies on having sufficiently abundant, accurate data and KANs (like MLPs) can struggle to train in the presence of noisy data [7, 8]. Also, compared to MLPs, KANs can struggle to train with sparse data [62, 63]. In this work, we introduce *multifidelity KANs* (MFKANs) which allow for training simultaneously with two datasets. MFKANs reduce the need for a large high-fidelity dataset by incorporating training with a second, low-fidelity dataset. We show that MFKANs can accurately learn linear and nonlinear correlations between the low- and high-fidelity datasets. In addition, MFKANs can be extended to physics-informed KANs [9], when no high-fidelity or low-fidelity data is available, but the physics governing the system is known.

2 Method

2.1 KANs

Kolmogorov-Arnold networks [4] approximate a multivariate function $f(\mathbf{x})$ by a model of the form

$$f(\mathbf{x}) \approx \sum_{i_{L-1}=1}^{n_{L-1}} \varphi_{L-1, i_L, i_{L-1}} \left(\sum_{i_{L-2}=1}^{n_{L-2}} \cdots \left(\sum_{i_2=1}^{n_2} \varphi_{2, i_3, i_2} \left(\sum_{i_1=1}^{n_1} \varphi_{1, i_2, i_1} \left(\sum_{i_0=1}^{n_0} \varphi_{0, i_1, i_0}(x_{i_0}) \right) \right) \right) \cdots \right), \quad (1)$$

inspired by the Kolmogorov-Arnold Theorem. L is the number of layers in the KAN, $\{n_j\}_{j=0}^L$ is the number of nodes per layer, and $\phi_{i,j,k}$ are the univariate activation functions. We denote the right-hand side of eq. (1) as $\mathcal{K}(x)$. The activation functions are represented (on a grid with g points) by a weighted combination of a basis function $b(x)$ and a B-spline,

$$\phi(x) = w_b b(x) + w_s \text{spline}(x), \quad (2)$$

where

$$b(x) = \frac{x}{1 + e^{-x}},$$

and

$$\text{spline}(x) = \sum_i c_i B_i(x).$$

Here, $B_i(x)$ is a polynomial of degree k . c_i , w_b , and w_s are trainable parameters if not predetermined by the user.

KANs evaluate the B-splines on a precomputed grid, which should align with the domain of the data. For example, in one dimension a domain $[a, b]$ with a grid with g_1 intervals has grid points $\{t_0 = a, t_1, t_2, \dots, t_{g_1} = b\}$; cf. [4]. In grid extension [4, 64] a new, fine-grained spline is fitted to a coarse-grained spline, increasing the expressivity of the KAN. The coarse splines are transferred to the fine splines following the procedure in [64]. The method in which the grid is selected has a significant impact on the training [64], although we leave a careful exploration of this topic for future work.

Single-fidelity KANs are trained to minimize the mean squared error (MSE) between the data and the prediction. For data-informed training we consider a dataset of labeled pairs $\{(x_i, f(x_i))\}_{i=1}^N$ and minimize the loss function

$$\mathcal{L}(\theta) = \frac{1}{N} \sum_{i=1}^N [\mathcal{K}(x_i; \theta) - f(x_i)]^2. \quad (3)$$

Here, θ is the set of trainable parameters. Physics-informed KANs (PIKANs) [9] have emerged as an alternative to physics-informed neural networks (PINNs) [65, 1, 66], where a physics-informed loss can be implemented in a manner analogous to PINNs [65]. We refer to recent work for a summary of PIKANs [9], and note that there are many recent extensions and variants [64, 67, 19, 68, 10, 69, 70].

2.2 Multifidelity KANs

In this work, we take inspiration from composite multifidelity neural networks [45], which consist of three MLPs. The first MLP learns a model of the low-fidelity training data. The second and third MLPs are added together to learn the correlation between the output of the low-fidelity model and the high-fidelity data, to provide an accurate prediction of the high-fidelity data. In particular, the second MLP learns the linear correlation between the low-fidelity model and the high-fidelity data, and the third MLP learns the nonlinear correlation. Ideally, the low-fidelity and high-fidelity datasets are highly correlated, so the linear correlation accounts for the bulk of the correlation, while the nonlinear correlation is a small correction. This structure allows for the nonlinear network to be smaller, increasing the robustness of training when only a small amount of high-fidelity data is available.

The foundations of multifidelity neural networks as presented in [45] translate well to multifidelity KANs (MFKANs). An MFKAN consists of three blocks: a low-fidelity KAN (\mathcal{K}_L), a linear KAN (\mathcal{K}_l), and a nonlinear KAN (\mathcal{K}_{nl}). The low-fidelity KAN learns a surrogate for the low-fidelity data or physics. Then, the output from the low-fidelity KAN is appended to the input parameters and passed as inputs to the linear and nonlinear KANs. The linear KAN learns the linear correlation between the input variables, the output of the low-fidelity KAN, and the high-fidelity data. The nonlinear KAN learns a nonlinear correction to the linear correlation, to account for general datasets which may not be strictly linearly correlated. An example of this structure is shown in Fig. 1.

We consider the case where we have two datasets, a low-fidelity dataset consisting of labeled pairs $\{(x_i, f_L(x_i))\}_{i=1}^{N_{LF}}$ and a high-fidelity dataset $\{(x_j, f_H(x_j))\}_{j=1}^{N_{HF}}$. Note that there is no requirement that $\{x_j\}_{j=1}^{N_{HF}}$ is a subset of $\{x_i\}_{i=1}^{N_{LF}}$. In the following sections, we provide some details on the specifics of each block.

2.2.1 Low-fidelity block

In general, the low-fidelity block can be a low-fidelity numerical model implemented directly, a standard KAN, or an MLP or other machine learning model. For the purposes of this work, we only consider KANs for the low-fidelity block except in Sec. 3.7, where we show an example of using a low-fidelity numerical model directly. The low-fidelity KAN is pretrained (as a single-fidelity KAN) using the low-fidelity data. The weights of the low-fidelity KAN are then frozen while training the high-fidelity networks. While training all networks simultaneously is possible, we found that it greatly increased the computational time.

The low-fidelity loss function with trainable parameters θ_L is given by

$$\mathcal{L}_L(\theta_L) = \frac{1}{N_{LF}} \sum_{i=1}^{N_{LF}} [\mathcal{K}_L(x_i; \theta_L) - f_L(x_i)]^2. \quad (4)$$

2.2.2 High-fidelity block

The high-fidelity prediction is a convex combination of the linear and nonlinear networks, given by

$$\mathcal{K}_H(\mathbf{x}) = \alpha \mathcal{K}_{nl}(\mathbf{x}) + (1 - \alpha) \mathcal{K}_l(\mathbf{x}), \quad (5)$$

where α is a trainable parameter. The high-fidelity loss function is modified to

$$\mathcal{L}_H(\theta_H, \alpha) = \frac{1}{N_{HF}} \sum_{j=1}^{N_{HF}} [\mathcal{K}_H(x_j; \theta_H) - f_H(x_j)]^2 + \lambda_\alpha \alpha^n + w \sum_{l=0}^{L-1} \|\Phi_{nl}\|, \quad (6)$$

where $\theta_H = \{\theta_{nl}, \theta_l\}$ is the set of trainable network parameters and n is a scalar, typically taken as $n = 4$. This minimizes α , which forces the method to learn the maximum linear correlation. If n is too small, forcing α to be smaller, the method may not learn the full nonlinear correlation, which reduces the expressivity of the method. If a strong nonlinear correlation is expected between the high-fidelity and low-fidelity data, it is possible to choose a larger value of n , although this training may require more high-fidelity data. λ_α is a parameter chosen before training. The set of trainable parameters θ_{HF} includes all trainable parameters of both the linear and nonlinear KANs. The final term in the loss function Eq. eq. (6) is the sum of the mean squared value of each KAN layer in the nonlinear network, inspired by [4] and given by

$$\|\Phi_{nl}\| = \frac{1}{n_{in} n_{out}} \sum_{i=1}^{n_{in}} \sum_{j=1}^{n_{out}} |\phi_{i,j}^{nl}|^2. \quad (7)$$

While [4] minimizes the L_1 norm to learn sparse solutions, here we use the minimization to prevent overfitting to possibly sparse high-fidelity data. We typically take $w = 0$ or $w = 1$, depending on any *a priori* known correlation between the low-fidelity and high-fidelity data.

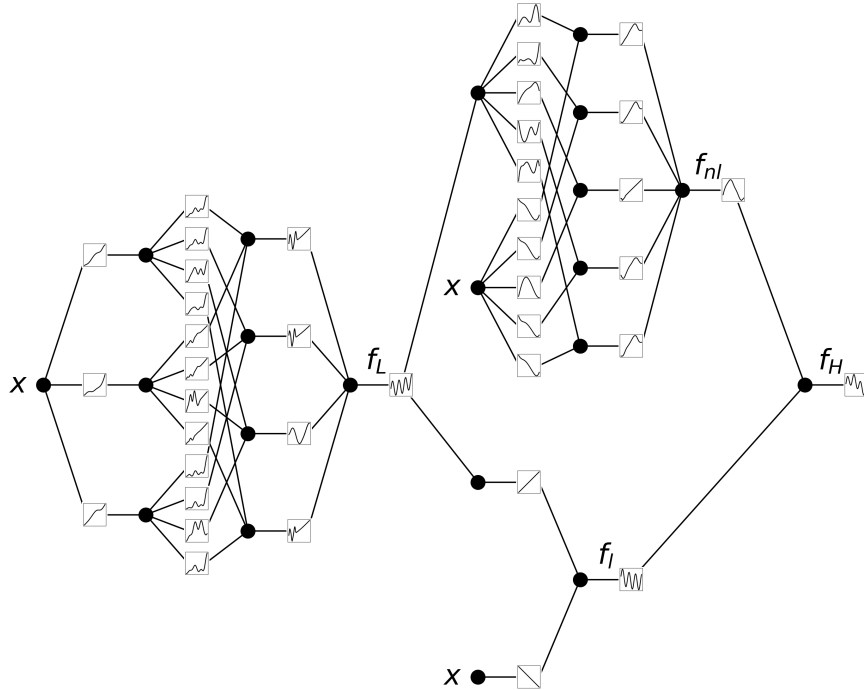


Figure 1: Example multifidelity KAN. The low-fidelity data is given by $f_L(x) = x^2 + \sin(20x)$ and $f_H(x) = f_L(x) - x + \sin(5x)$ for $x \in [0, 1]$. It is evident that the linear KAN learns the linear correlations and the nonlinear KAN outputs the nonlinear correlation ($\sin(5x)$).

2.2.3 Linear block

A linear correlation is a first-degree polynomial, which makes this block easy to implement as a KAN by taking the polynomial degree of the basis as $k = 1$. We also must take $w_b = 0$ and $w_s = 1$ in Eq. 2. We use only two grid points (*i.e.*, $g_1 = 1$ so $t_0 = a$ and $t_1 = b$). This allows learning a global linear correlation that is constant across the full domain. For all examples in this work, the linear block does not contain a hidden layer.

KANs do offer additional flexibility over MLPs, though. If it is known that the low-fidelity data and the high-fidelity data are linearly correlated, but with different correlations in different parts of the domain, we could increase the number of grid points to learn additional linear correlations. Ideally, the grid points should correspond with the boundaries of the domains of each of the known linear correlations. We leave an exploration of this idea for future work.

2.2.4 Nonlinear block

The nonlinear block is a standard KAN of degree $k > 1$. We still take $w_s = 1$ in Eq. 2, as we find this improves the training (w_b is a trainable parameter.)

2.2.5 Implementation

For the examples listed in this paper, the code is implemented in Jax [71], using the jaxKAN package [72, 64].

To report errors we consider the relative ℓ_2 error, given by

$$\frac{\|\mathcal{K}_i(x; \theta_i) - f_j(x)\|_2}{\|f_j(x)\|_2} \quad (8)$$

where i and j denote either low-fidelity or high-fidelity.

3 Results

3.1 Test 1: Jump function with a linear correlation

We begin by considering a jump function with a linear correlation. In this example, we have sparse high-fidelity data, which is not sufficient to capture the jump.

$$f_L(x) = \begin{cases} 0.1 [0.5(6x - 2)^2 \sin(12x - 4) + 10(x - 0.5) - 5] & x \leq 0.5, \\ 0.1 [0.5(6x - 2)^2 \sin(12x - 4) + 10(x - 0.5) - 2] & x > 0.5, \end{cases} \quad (9)$$

$$f_H(x) = 2f_L(x) - 2x + 2, \quad (10)$$

for $x \in [0, 1]$. We take $N_{LF} = 50$ low-fidelity data points evenly distributed in $[0, 1]$ and $N_{HF} = 5$ high-fidelity data points evenly spaced in $[0.1, 0.93]$. Results are shown in Fig. 2 and Fig. 3.

We first consider training only on high-fidelity data. Although the network trains to a very small MSE on the high-fidelity training data ($< 10^{-15}$) (Fig. 2b), the resulting prediction has a large relative ℓ_2 error of 0.307 because of the sparsity of the high-fidelity data. We then consider the multifidelity training with $w = 0$ and $w = 1$. One thing to note is that the low-fidelity prediction, even with the large amount of low-fidelity data, struggles to capture the jump accurately. This could be due to the B-splines used in the KANs basis having to interpolate the jump. The relative ℓ_2 error of the low-fidelity prediction is 0.0231. The high-fidelity predictions have very similar relative ℓ_2 errors, of 0.0651 and 0.0571 for $w = 0$ and $w = 10$, respectively. Even with sparse high-fidelity data, the multifidelity prediction is able to accurately capture the jump.

To better understand how the error in the low-fidelity predictions due to having discrete data is propagated through to the multifidelity predictions, we consider a separate test with $N_{LF} = 300$, shown in Fig. 3. With the additional low-fidelity data, the relative ℓ_2 error of the low-fidelity prediction drops to 0.0054, approximately a factor of four. The multifidelity predictions drop by a corresponding amount, to 0.0105 for $w = 0$ and 0.0102 for $w = 10$.

3.2 Test 2: Nonlinear correlation

We next test a nonlinear correlation between the low-fidelity and high-fidelity data, taken from [45]. The equations for the low- and high-fidelity data are given by:

$$f_L(x) = \sin(8\pi x), \quad (11)$$

$$f_H(x) = (x - \sqrt{2}) \sin^2(8\pi x), \quad (12)$$

We take $N_{LF} = 51$ and $N_{HF} = 14$ on $[0, 1]$. Results are shown in Fig. 4. When $w = 0$, the nonlinear correlation suffers from overfitting the sparse high-fidelity data, which is shown in Fig. 4e. When $w = 1$, the overfitting is reduced. Clearly, training with only the high-fidelity data in Fig. 4f does not accurately capture the high-fidelity reference.

3.3 Test 3: two-dimensional nonlinear correlation

To further test the method, we turn to a nonlinear correlation in two dimensions, given by

$$f_L(x, y) = \sin(12\pi x), \quad (13)$$

$$f_H(x, y) = 2f_L(x, y) + \sin(12y), \quad (14)$$

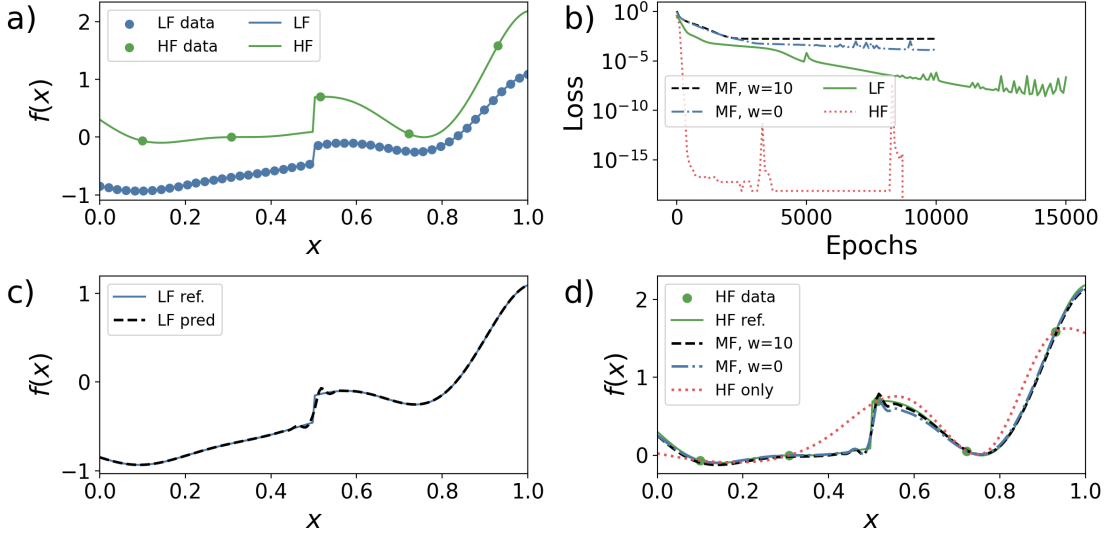


Figure 2: Results for Test 1 with $N_{LF} = 50$. a) Plotted low- and high-fidelity data points and functions for reference. b) Loss values for multifidelity, low-fidelity, and high-fidelity training. c) Low-fidelity reference function and low-fidelity prediction. d) High-fidelity reference function and multifidelity and high-fidelity predictions.

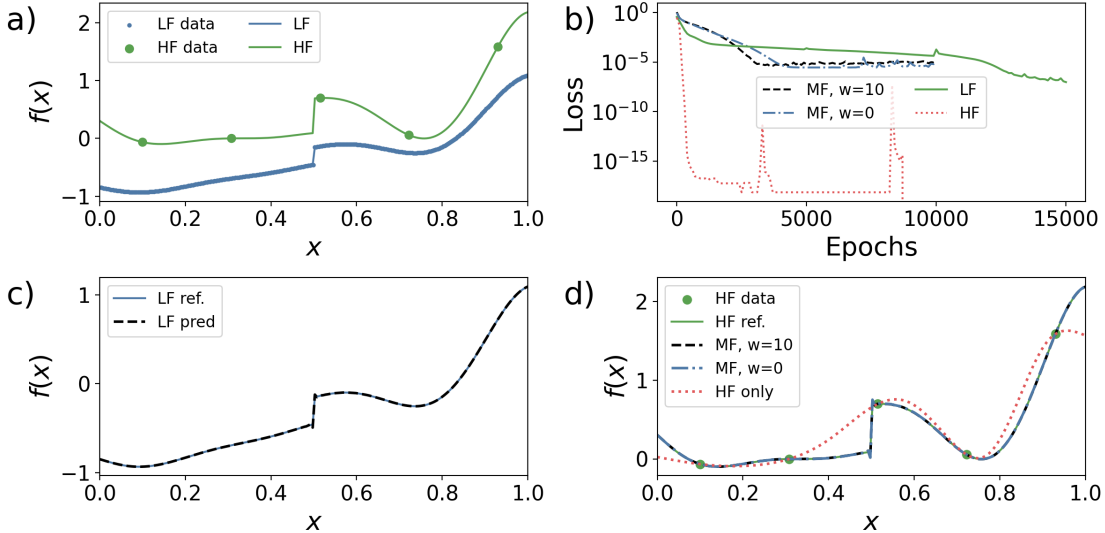


Figure 3: Results for Test 1 with $N_{LF} = 300$. a) Plotted low- and high-fidelity data points and functions for reference. b) Loss values for multifidelity, low-fidelity, and high-fidelity training. c) Low-fidelity reference function and low-fidelity prediction. d) High-fidelity reference function and multifidelity and high-fidelity predictions.

for $x, y \in [0, 1] \times [0, 1]$. The low-fidelity data is selected on a 100×100 mesh, so $N_{LF} = 10^4$. The high-fidelity data is selected on a 10×15 mesh, with $N_{HF} = 150$. The high-fidelity data locations are shown in Fig. 5a.

Plots of the high-fidelity and multifidelity predictions of the high-fidelity data are given in Fig. 5c and d. Without the low-fidelity data, the high-fidelity prediction is unable to capture the high-frequency oscillations in the x -direction. In contrast, the multifidelity prediction agrees well with the reference solution. The full plots of the solutions are given in Fig. 6. The multifidelity prediction has a much smaller absolute error than the high-fidelity prediction (Fig. 6, right column.) The relative ℓ_2 error of the low-fidelity prediction is 0.0033, and the relative ℓ_2 errors of the multifidelity and high-fidelity predictions are 0.0201 and 0.9641, respectively.

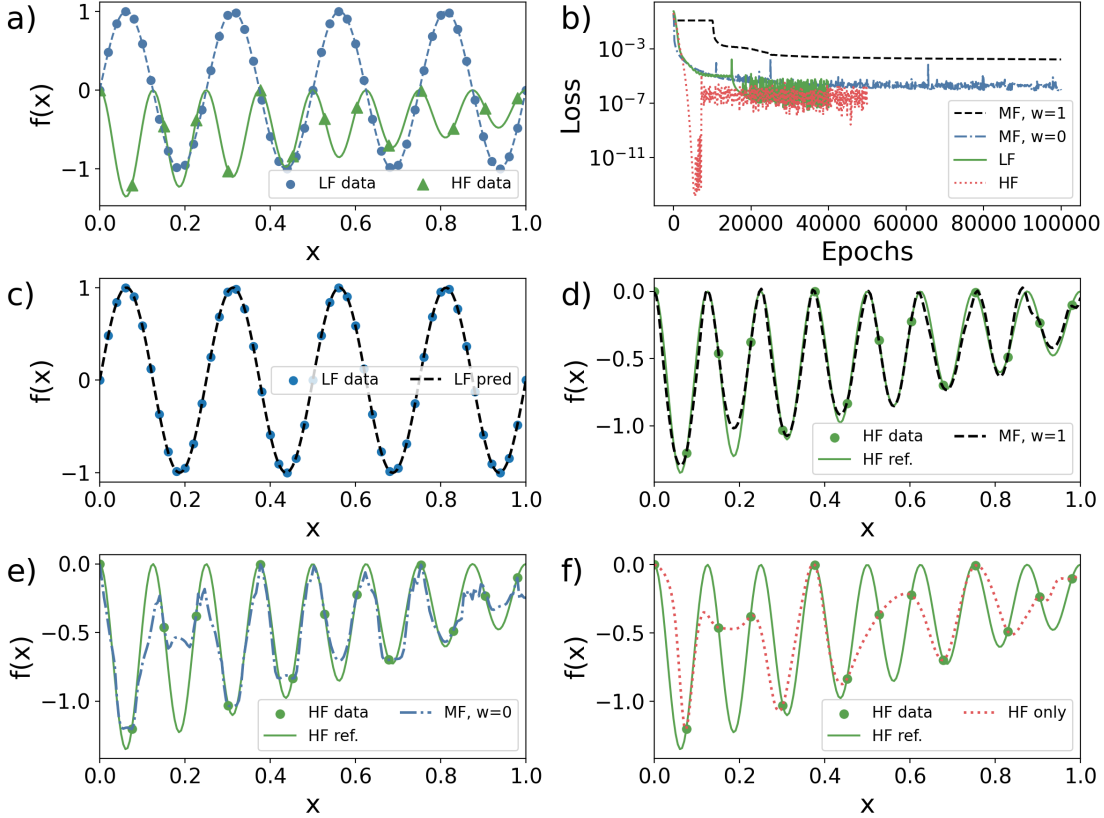


Figure 4: Results for Test 2. a) Reference solutions and training data. b) Loss curves for single-fidelity and multifidelity training. c) Low-fidelity reference solution and prediction. d) High-fidelity reference solution and multifidelity prediction with $w = 1$. e) High-fidelity reference solution and multifidelity prediction with $w = 0$. f) High-fidelity reference solution and high-fidelity prediction.

3.4 Test 4: Higher-dimensional problem

We now turn to a higher-dimensional problem:

$$f_L(x_1, x_2, x_3, x_4) = 1.2f_H(x_1, x_2, x_3, x_4) - 0.5, \quad (15)$$

$$f_H(x_1, x_2, x_3, x_4) = 0.5(0.1 \exp(x_1 + x_2) - x_4 \sin(12\pi x_3) + x_3), \quad (16)$$

for $x_i \in [0, 1]$, $i = 1, 2, 3, 4$. To further test the method, we also consider a case with Gaussian white noise added to both the low-fidelity and high-fidelity training data. The variance of the noise is denoted by σ_L and σ_H for the low- and high-fidelity samples, respectively. To generate the training data we take $N_{LF} = 25,000$ and $N_{HF} = 150$ and sample the training points randomly in $\Omega = [0, 1]^4$. We show the results of training in Table 1 and Fig. 7. The high-fidelity predictions have large relative errors and are not able to capture the true solution. In contrast, the multifidelity predictions are much more accurate, even in the presence of noisy data. The errors do increase somewhat when noise is added to the training data.

| | LF | MF | HF |
|------------------------------------|--------|--------|--------|
| $\sigma_L = 0, \sigma_H = 0$ | 0.0207 | 0.0110 | 0.5046 |
| $\sigma_L = 0.05, \sigma_H = 0.03$ | 0.0408 | 0.0301 | 0.5297 |

Table 1: Relative ℓ_2 errors for Test 4.

3.5 Test 5: Physics-informed training

Physics-informed KANs (PIKANs) have attracted recent attention [64, 67, 9, 10, 68, 69, 73]. PIKANs use the basic ideas of physics-informed neural networks (PINNs) [65], but with KANs instead of MLPs as the neural architecture.

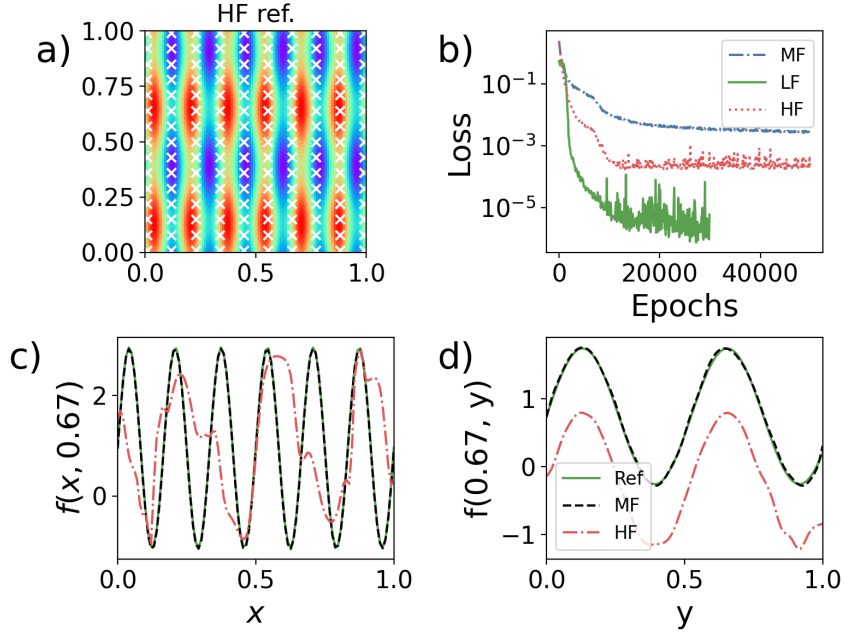


Figure 5: Results for Test 3. a) Depiction of the high-fidelity data locations. b) Loss curves for low-fidelity, high-fidelity, and multifidelity training. c) Trained predictions along the line $y = 0.67$. d) Trained predictions along the line $x = 0.67$.

One can consider many cases in which physics-informed training could be useful within a multifidelity framework. Perhaps the available data is on a coarse mesh but the physics of the system is known. In this case, physics-informed training can be used instead of high-fidelity data to perform something akin to super-resolution (*e.g.*, [74, 75, 76, 77, 42]). In other cases, a small amount of high-fidelity data may be available, as well as low-order physics-based models. In these cases, we can use physics instead of the low-fidelity data, which is then corrected with the high-fidelity data. A third use case arises from the observations in [9, 64, 68] that PIKANs can be difficult to train. In practice, single-fidelity PIKANs can fail to accurately capture the true solution of the equation used to train the KAN. In these cases, we can use physics at both levels of the multifidelity training, to correct a solution that is learned with too high an error, along the lines of iteratively learning a solution that has recently become popular for PINNs [46, 78, 79, 80, 81]. It is an example of this form that we consider in this section.

We consider the Poisson equation

$$\frac{d^2 u}{dx^2} = f(x), \quad x \in [0, 1], \quad (17)$$

$$u(0) = u(1) = 0, \quad (18)$$

with exact solution $u(x) = \sin(2k\pi x^2)$, which determines $f(x)$. For the target high-fidelity equation we use $k = 12$, and for the low-fidelity we use $k = 4$. In this case we train without data, and instead use a physics-informed loss function [65]. Results are shown in Fig. 8. The high-fidelity KAN attempts to predict the solution to the Poisson equation with $k = 12$. However, it has a large relative ℓ_2 error of 0.346. In contrast, the multifidelity prediction predicts the low-fidelity reference solution with a relative error of 0.0153, and the high-fidelity reference solution with a relative error of 0.0221.

3.6 Test 6: Mechanical MNIST

We consider the multifidelity Mechanical MNIST dataset [82, 83]. The dataset is created by applying uniaxial extension to materials created from MNIST [84]. We consider two meshes as our low- and high-fidelity data. The high-fidelity dataset has a fully refined mesh with quadratic triangular elements (denoted by UE in [37]). The low-fidelity dataset is generated using $14 \times 14 \times 2$ linear triangular elements (UE-CM-14). We train with the 60,000 samples from the low-fidelity training set, and N samples from the high-fidelity dataset. Then, we test with 10,000 samples from the low- and high-fidelity datasets.

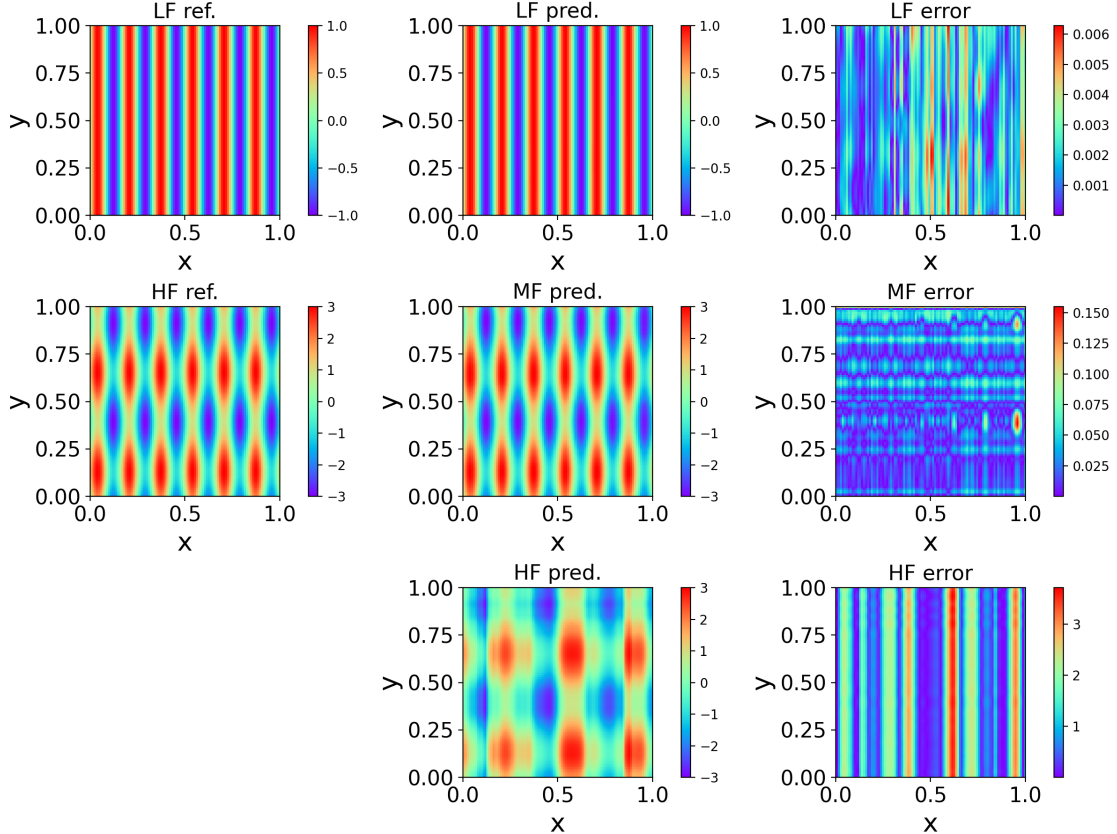


Figure 6: Results for Test 3. Top row: low-fidelity reference solution and prediction. Middle row: multifidelity reference solution and prediction. Bottom row: high-fidelity prediction.

The goal is to predict the total change in strain energy when the block is stretched to 50% of its original length, denoted by $\nabla\psi$. From [83], the high-fidelity mechanical MNIST dataset trained with an MLP results a mean percent error (MPE) of 2.5% when trained with the entire high-fidelity dataset [83] and the MPE is reduced to 1.0% with a convolutional neural network (CNN) [37] (we emphasize that we use the MPE instead of the relative ℓ_2 error in this section to align with [83]). Using transfer learning with a low-fidelity dataset can further reduce the MSE and reduce the amount of high-fidelity data needed to train [37].

We first test the training of the KAN on the mechanical MNIST high-fidelity dataset to compare the MPE between MLPs and KANs. We note that while CNNs have shown better performance for MNIST, a multifidelity convolutional KAN extending [17] is outside the scope of this work. As a baseline, the KAN trained with the entire high-fidelity dataset achieves an MPE of 1.26%.

The low-fidelity model has an MPE of 1.60% on the low-fidelity test set and 8.53% on the high-fidelity test set. Clearly, the low-fidelity KAN is a good model for the low-fidelity test set, but it does not accurately predict the high-fidelity data. We test the high-fidelity KAN and MFKAN by varying the size of the high-fidelity training set from 200 to 60,000. As shown in Fig. 9b, the MFKAN has a lower test MPE than the high-fidelity KAN in all cases except when trained with the full training set with 60,000 samples. This demonstrates that in the presence of limited high-fidelity data, the MFKAN can outperform a KAN trained with only high-fidelity data.

3.7 Test 7: Multifidelity extrapolation

To test our multifidelity method with a more realistic application, we consider the case of developing a surrogate for an expensive numerical code. Neural architectures, in general, struggle with extrapolation, or predictions outside the domain of input values. This means that for models trained with numerical data, we must have numerical data spanning the entire time range at which we want predictions, which can be very expensive to produce. In this section, we demonstrate that we can successfully extrapolate beyond our high-fidelity data if we have a low-fidelity numerical code for generating low-fidelity data.

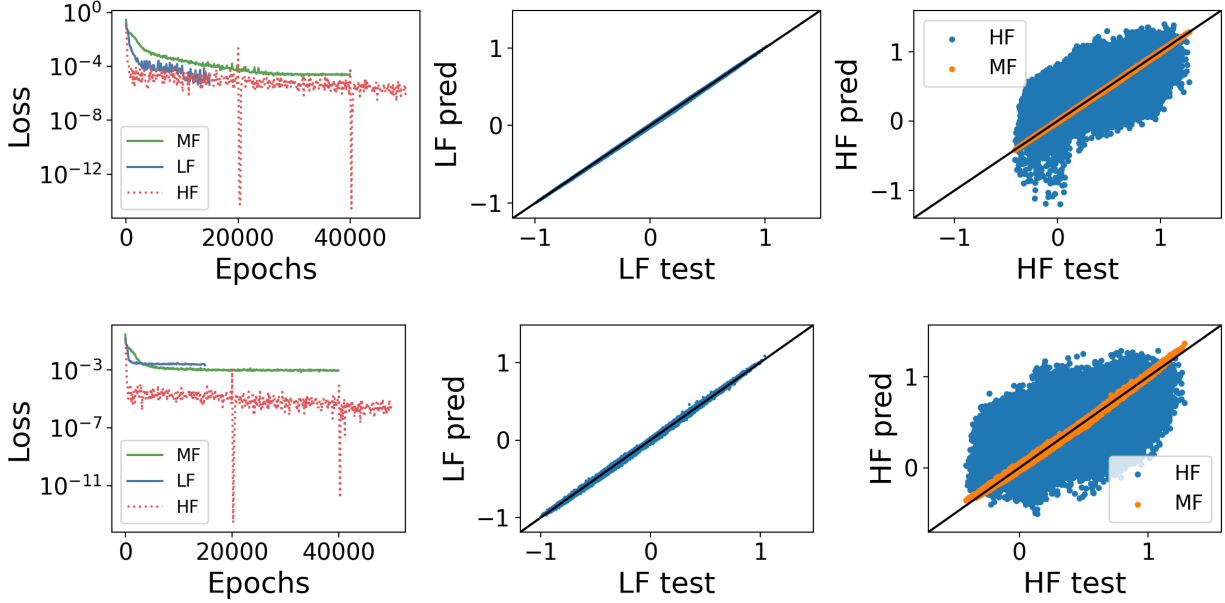


Figure 7: Results for Test 4 with clean data (top) and noisy data (bottom). Noisy data has white noise with variance $\sigma_L = 0.05$ added to the low-fidelity data and $\sigma_H = 0.03$ added to the high-fidelity data. Left to right: loss curves, low-fidelity prediction, and high-fidelity prediction.

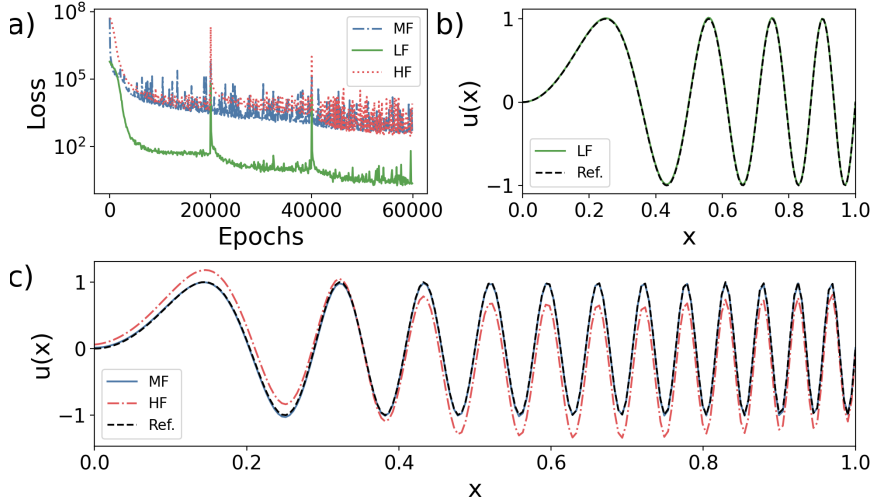


Figure 8: Results for Test 5. a) Loss curves. b) Low-fidelity reference solution and prediction. c) High-fidelity reference solution and predictions.

Specifically, we consider the vorticity field of a fluid flow past a cylinder generated with Phi Flow [85] to match the Wake Flow tutorial. The dimensionless domain is $\Omega = [0, 200] \times [0, 100]$, with a cylinder of radius 10 located at $(20, 50)$. For the high-fidelity data, we use a 257×129 mesh. We select 200 consecutive time steps after the unsteady flow has developed. For the low-fidelity data, we sub-sample the high-fidelity mesh to create a 86×43 mesh, keeping the same time steps. Importantly, we train with all the low-fidelity data and only the first 100 timesteps of the high-fidelity data. This means that when predicting for $t > 100$, the model is extrapolating in time with respect to the high-fidelity data.

Instead of training a single-fidelity KAN for the low-fidelity data, we directly use our numerical solver to generate the low-fidelity input to the multifidelity network. This reduces the error that can occur due to the low-fidelity prediction.

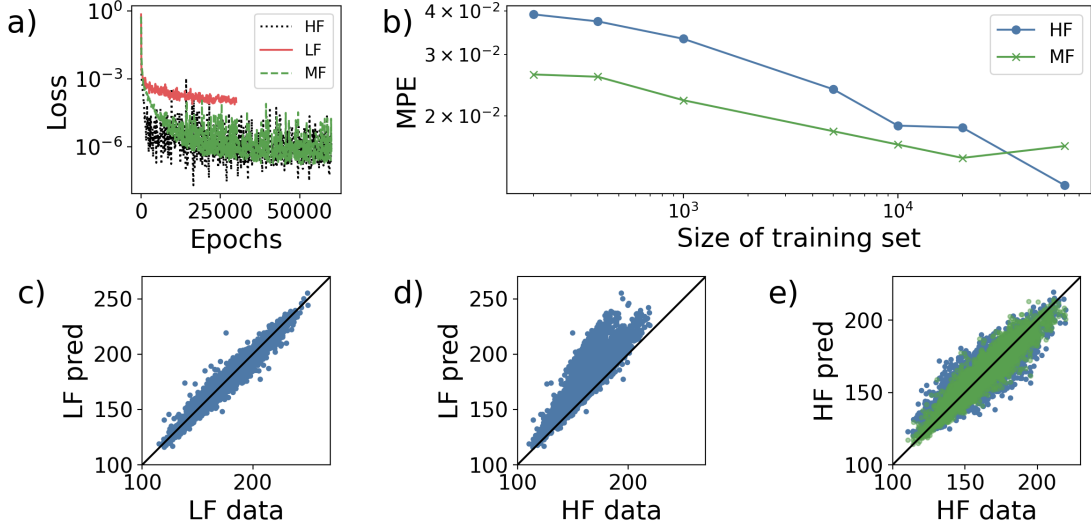


Figure 9: Results for Test 6. a) Loss curves. b) MPE for both MFKAN and high-fidelity KAN tests. c) LF predictions of the LF data compared with reference LF data. d) LF predictions of the HF data, compared with reference HF data. e) HF predictions of the HF data, compared with reference HF data for the high-fidelity KAN (blue) and the MFKAN (green).

In Figure 10b we show the relative ℓ_2 error over time for the multifidelity and high-fidelity predictions. In the area where there is no high-fidelity data, $t \in [100, 200]$, the high-fidelity relative ℓ_2 error is significantly higher, after jumping rapidly at $t = 100$. In contrast, the multifidelity error increases only slightly in the extrapolation region and does not grow substantially with time. The multifidelity model has a significantly lower error than just interpolating the low-fidelity data to the high-fidelity mesh.

In Figs. 11 and 12 we show sample outputs from the simulations and model predictions. Fig. 11 contains two dimensionless time snapshots for the time domain where high-fidelity data is provided. Both models are able to capture the high-fidelity simulation data, although the high-fidelity model does have slightly higher accuracy. Fig. 12 has two snapshots in the extrapolation region. The single-fidelity solution no longer captures the vortex structure accurately. In contrast, the multifidelity model remains accurate at $t = 200$.

This example shows the potential power of multifidelity modeling for reducing the computational cost of generating data for machine-learned surrogates. While a small amount of high-fidelity data is still necessary, the model can extrapolate forward in time given only additional low-fidelity data, which is less expensive to produce.

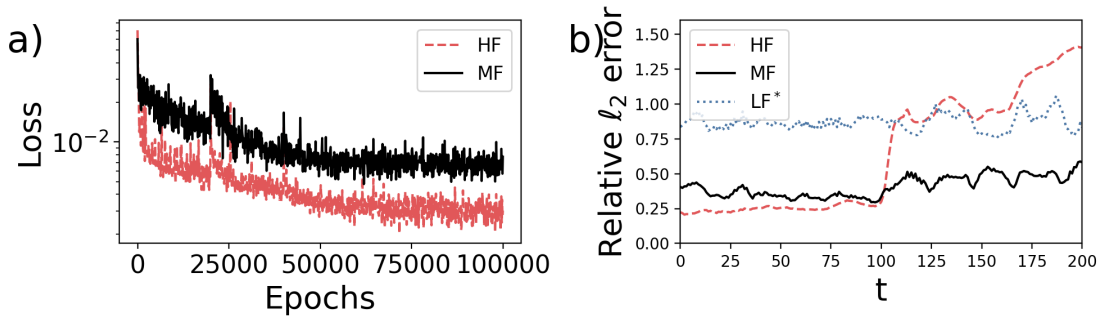


Figure 10: Results for Test 7. a) Loss curves. b) Relative ℓ_2 error over time for the high-fidelity and multifidelity predictions. The low-fidelity error is the error of the low-fidelity data extrapolated to the high-fidelity mesh.

4 Conclusions

We have developed an adaptable, robust framework for multifidelity modeling with KANs. Our method takes advantage of the B-splines learned in KANs to learn the nonlinear and linear correlations between the low- and high-fidelity datasets. In particular, this method does not require a nested dataset (that is, the high-fidelity dataset does not need to be a subset of the low-fidelity dataset) because a low-fidelity KAN is trained on the low-fidelity dataset, which then serves as a surrogate for the low-fidelity data. This flexibility allows the method to be adapted to a variety of complex applications, where nested datasets may not be available.

As noted in the introduction, the field of training KANs has been rapidly changing, with many variations being added weekly and monthly. We note that the multifidelity framework presented here does not rely on KANs as implemented in [4]. In particular, the nonlinear and low-fidelity blocks can be replaced by KAN variants as they emerge, including recent advances in different basis functions [16, 86, 70, 87, 88]. Additionally, the flexibility of the method allows for different network types to be used for each block to best fit the data. For instance, an MLP could be used for the low-fidelity data and a KAN for the nonlinear network. This flexibility presents opportunities for adapting the framework for the best performance as KANs continue to develop and for modifying the method to best fit the characteristics of a given dataset.

5 Data and code availability

The Mechanical MNIST dataset in Sec. 3.6 is available at [82]. The fluid flow data in Sec. 3.7 was produced with [85]. The KANs results in this work were produced with code adapted from JaxKAN [72, 64]. All code and data will be released upon publication in a journal. For those wishing to implement the method themselves, tutorials for some examples are available in Neuromancer [89] at <https://github.com/pnnl/neuromancer/blob/feature/mfkans/examples/KANs/>. Training parameters used to train the results in this paper are given in Sec. A.

6 Acknowledgements

The code to plot the KAN diagrams in the graphical abstract and fig. 1 was adapted from pykan [4].

This project was completed with support from the U.S. Department of Energy, Advanced Scientific Computing Research program, under the Scalable, Efficient and Accelerated Causal Reasoning Operators, Graphs and Spikes for Earth and Embedded Systems (SEA-CROGS) project (Project No. 80278) and under the Uncertainty Quantification for Multifidelity Operator Learning (MOLUcQ) project (Project No. 81739). The computational work was performed using PNNL Institutional Computing at Pacific Northwest National Laboratory. Pacific Northwest National Laboratory (PNNL) is a multi-program national laboratory operated for the U.S. Department of Energy (DOE) by Battelle Memorial Institute under Contract No. DE-AC05-76RL01830.

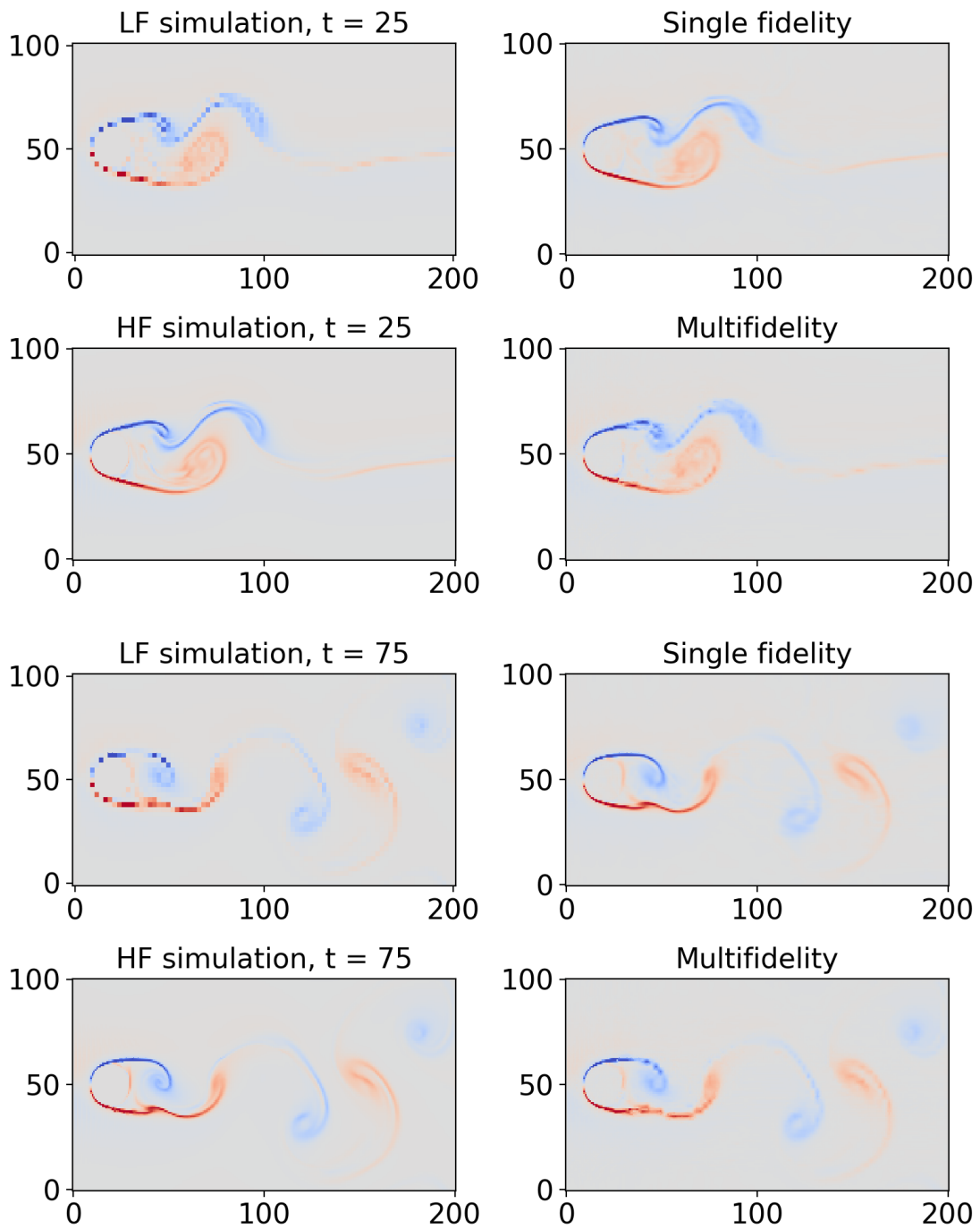


Figure 11: Results for Test 7 in the time-extrapolation domain at $t = 25$ and $t = 75$. Top left: low-fidelity simulation output. Bottom left: high-fidelity simulation output. Top right: single-fidelity prediction. Bottom right: multifidelity prediction.

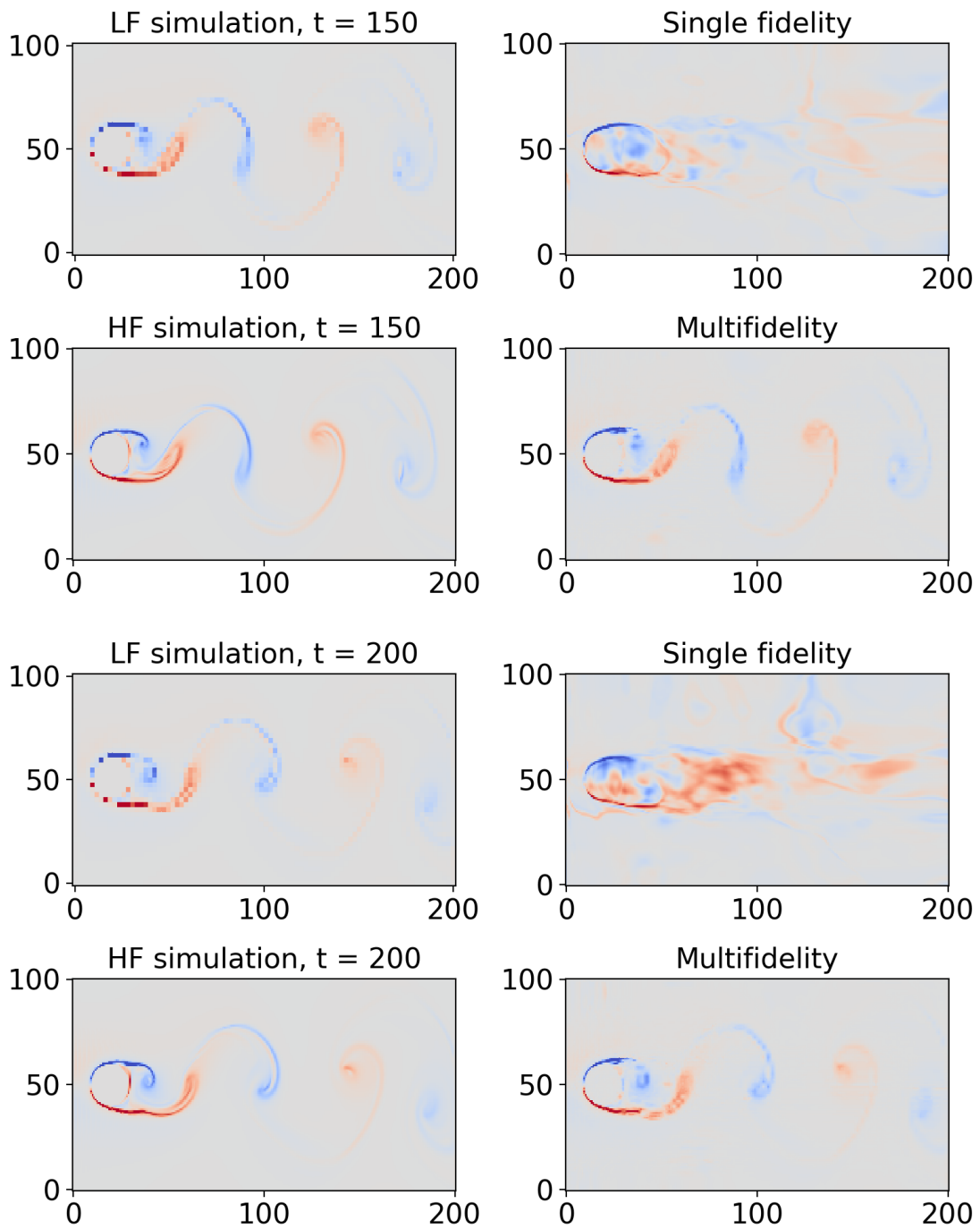


Figure 12: Results for Test 7 in the time-extrapolation domain at $t = 150$ and $t = 200$. Top left: low-fidelity simulation output. Bottom left: high-fidelity simulation output. Top right: single-fidelity prediction. Bottom right: multifidelity prediction.

References

- [1] George Em Karniadakis, Ioannis G Kevrekidis, Lu Lu, Paris Perdikaris, Sifan Wang, and Liu Yang. Physics-informed machine learning. *Nature Reviews Physics*, 3(6):422–440, 2021.
- [2] Nathan Baker, Frank Alexander, Timo Bremer, Aric Hagberg, Yannis Kevrekidis, Habib Najm, Manish Parashar, Abani Patra, James Sethian, Stefan Wild, et al. Workshop report on basic research needs for scientific machine learning: Core technologies for artificial intelligence. Technical report, USDOE Office of Science (SC), Washington, DC (United States), 2019.
- [3] Jonathan Carter, John Feddema, Doug Kothe, Rob Neely, Jason Pruet, Rick Stevens, Prasanna Balaprakash, Pete Beckman, Ian Foster, Kamil Iskra, et al. Advanced research directions on ai for science, energy, and security: Report on summer 2022 workshops. 2023.
- [4] Ziming Liu, Yixuan Wang, Sachin Vaidya, Fabian Ruele, James Halverson, Marin Soljačić, Thomas Y Hou, and Max Tegmark. Kan: Kolmogorov-arnold networks. *arXiv preprint arXiv:2404.19756*, 2024.
- [5] Ziming Liu, Pingchuan Ma, Yixuan Wang, Wojciech Matusik, and Max Tegmark. Kan 2.0: Kolmogorov-arnold networks meet science. *arXiv preprint arXiv:2408.10205*, 2024.
- [6] Runpeng Yu, Weihao Yu, and Xinchao Wang. Kan or mlp: A fairer comparison. *arXiv preprint arXiv:2407.16674*, 2024.
- [7] Chen Zeng, Jiahui Wang, Haoran Shen, and Qiao Wang. Kan versus mlp on irregular or noisy functions. *arXiv preprint arXiv:2408.07906*, 2024.
- [8] Haoran Shen, Chen Zeng, Jiahui Wang, and Qiao Wang. Reduced effectiveness of kolmogorov-arnold networks on functions with noise. *arXiv preprint arXiv:2407.14882*, 2024.
- [9] Khemraj Shukla, Juan Diego Toscano, Zhicheng Wang, Zongren Zou, and George Em Karniadakis. A comprehensive and fair comparison between mlp and kan representations for differential equations and operator networks. *arXiv preprint arXiv:2406.02917*, 2024.
- [10] Yizheng Wang, Jia Sun, Jinshuai Bai, Cosmin Anitescu, Mohammad Sadegh Eshaghi, Xiaoying Zhuang, Timon Rabczuk, and Yinghua Liu. Kolmogorov arnold informed neural network: A physics-informed deep learning framework for solving pdes based on kolmogorov arnold networks. *arXiv preprint arXiv:2406.11045*, 2024.
- [11] Remi Genet and Hugo Inzirillo. Tkan: Temporal kolmogorov-arnold networks. *arXiv preprint arXiv:2405.07344*, 2024.
- [12] Zavareh Bozorgasl and Hao Chen. Wav-kan: Wavelet kolmogorov-arnold networks. *arXiv preprint arXiv:2405.12832*, 2024.
- [13] Mehrdad Kiamari, Mohammad Kiamari, and Bhaskar Krishnamachari. Gkan: Graph kolmogorov-arnold networks. *arXiv preprint arXiv:2406.06470*, 2024.
- [14] Gianluca De Carlo, Andrea Mastropietro, and Aris Anagnostopoulos. Kolmogorov-arnold graph neural networks, 2024.
- [15] Roman Bresson, Giannis Nikolentzos, George Panagopoulos, Michail Chatzianastasis, Jun Pang, and Michalis Vazirgiannis. Kagnns: Kolmogorov-arnold networks meet graph learning, 2024.
- [16] Sidharth SS. Chebyshev polynomial-based kolmogorov-arnold networks: An efficient architecture for nonlinear function approximation. *arXiv preprint arXiv:2405.07200*, 2024.
- [17] Alexander Dylan Bodner, Antonio Santiago Tepsich, Jack Natan Spolski, and Santiago Pourteau. Convolutional kolmogorov-arnold networks. *arXiv preprint arXiv:2406.13155*, 2024.
- [18] Qi Qiu, Tao Zhu, Helin Gong, Liming Chen, and Huansheng Ning. Relu-kan: New kolmogorov-arnold networks that only need matrix addition, dot multiplication, and relu. *arXiv preprint arXiv:2406.02075*, 2024.
- [19] Chi Chiu So and Siu Pang Yung. Higher-order-relu-kans (hrkans) for solving physics-informed neural networks (pinns) more accurately, robustly and faster. *arXiv preprint arXiv:2409.14248*, 2024.
- [20] Alireza Afzal Aghaei. fkan: Fractional kolmogorov-arnold networks with trainable jacobi basis functions. *arXiv preprint arXiv:2406.07456*, 2024.
- [21] Amanda A Howard, Bruno Jacob, Sarah H Murphy, Alexander Heinlein, and Panos Stinis. Finite basis kolmogorov-arnold networks: domain decomposition for data-driven and physics-informed problems. *arXiv preprint arXiv:2406.19662*, 2024.
- [22] Diab W Abueidda, Panos Pantidis, and Mostafa E Mobasher. Deepokan: Deep operator network based on kolmogorov arnold networks for mechanics problems. *arXiv preprint arXiv:2405.19143*, 2024.

- [23] Juan Diego Toscano, Theo Käufer, Martin Maxey, Christian Cierpka, and George Em Karniadakis. Inferring turbulent velocity and temperature fields and their statistics from lagrangian velocity measurements using physics-informed kolmogorov-arnold networks. *arXiv preprint arXiv:2407.15727*, 2024.
- [24] Ali Kashefi. Kolmogorov-arnold pointnet: Deep learning for prediction of fluid fields on irregular geometries. *arXiv preprint arXiv:2408.02950*, 2024.
- [25] Cristian J Vaca-Rubio, Luis Blanco, Roberto Pereira, and Mărius Caus. Kolmogorov-arnold networks (kans) for time series analysis. *arXiv preprint arXiv:2405.08790*, 2024.
- [26] Minjong Cheon. Kolmogorov-arnold network for satellite image classification in remote sensing. *arXiv preprint arXiv:2406.00600*, 2024.
- [27] Zhaojing Huang, Jiashuo Cui, Leping Yu, Luis Fernando Herbozo Contreras, and Omid Kavehei. Abnormality detection in time-series bio-signals using kolmogorov-arnold networks for resource-constrained devices. *medRxiv*, pages 2024–06, 2024.
- [28] Basim Azam and Naveed Akhtar. Suitability of kans for computer vision: A preliminary investigation. *arXiv preprint arXiv:2406.09087*, 2024.
- [29] Minjong Cheon. Demonstrating the efficacy of kolmogorov-arnold networks in vision tasks. *arXiv preprint arXiv:2406.14916*, 2024.
- [30] Yuki Nagai and Masahiko Okumura. Kolmogorov–arnold networks in molecular dynamics. *arXiv preprint arXiv:2407.17774*, 2024.
- [31] M Giselle Fernández-Godino. Review of multi-fidelity models. *arXiv preprint arXiv:1609.07196*, 2016.
- [32] Benjamin Peherstorfer, Karen Willcox, and Max Gunzburger. Survey of multifidelity methods in uncertainty propagation, inference, and optimization. *Siam Review*, 60(3):550–591, 2018.
- [33] Michael Penwarden, Shandian Zhe, Akil Narayan, and Robert M Kirby. Multifidelity modeling for physics-informed neural networks (PINNs). *Journal of Computational Physics*, 451:110844, 2022.
- [34] Dong H Song and Daniel M Tartakovsky. Transfer learning on multifidelity data. *Journal of Machine Learning for Modeling and Computing*, 3(1), 2022.
- [35] Souvik Chakraborty. Transfer learning based multi-fidelity physics informed deep neural network. *Journal of Computational Physics*, 426:109942, 2021.
- [36] Adrienne M. Propp and Daniel M. Tartakovsky. Transfer learning on multi-dimensional data: A novel approach to neural network-based surrogate modeling, 2024.
- [37] Emma Lejeune and Bill Zhao. Exploring the potential of transfer learning for metamodels of heterogeneous material deformation. *Journal of the Mechanical Behavior of Biomedical Materials*, 117:104276, 2021.
- [38] Zengcong Li, Shu Zhang, Hongqing Li, Kuo Tian, Zhizhong Cheng, Yan Chen, and Bo Wang. On-line transfer learning for multi-fidelity data fusion with ensemble of deep neural networks. *Advanced Engineering Informatics*, 53:101689, 2022.
- [39] Subhayan De and Alireza Doostan. Neural network training using ℓ_1 -regularization and bi-fidelity data. *Journal of Computational Physics*, 458:111010, 2022.
- [40] Su Jiang and Louis J Durlofsky. Use of multifidelity training data and transfer learning for efficient construction of subsurface flow surrogate models. *Journal of Computational Physics*, 474:111800, 2023.
- [41] Subhayan De, Jolene Britton, Matthew Reynolds, Ryan Skinner, Kenneth Jansen, and Alireza Doostan. On transfer learning of neural networks using bi-fidelity data for uncertainty propagation. *International Journal for Uncertainty Quantification*, 10(6), 2020.
- [42] Maryam Aliakbari, Mostafa Mahmoudi, Peter Vadasz, and Amirhossein Arzani. Predicting high-fidelity multi-physics data from low-fidelity fluid flow and transport solvers using physics-informed neural networks. *International Journal of Heat and Fluid Flow*, 96:109002, 2022.
- [43] Mengwu Guo, Andrea Manzoni, Maurice Amendt, Paolo Conti, and Jan S Hesthaven. Multi-fidelity regression using artificial neural networks: Efficient approximation of parameter-dependent output quantities. *Computer methods in applied mechanics and engineering*, 389:114378, 2022.
- [44] Wenqian Chen and Panos Stinis. Feature-adjacent multi-fidelity physics-informed machine learning for partial differential equations. *arXiv preprint arXiv:2303.11577*, 2023.
- [45] Xuhui Meng and George Em Karniadakis. A composite neural network that learns from multi-fidelity data: Application to function approximation and inverse PDE problems. *Journal of Computational Physics*, 401:109020, 2020.

- [46] Amanda A Howard, Sarah H Murphy, Shady E Ahmed, and Panos Stinis. Stacked networks improve physics-informed training: applications to neural networks and deep operator networks. *arXiv preprint arXiv:2311.06483*, 2023.
- [47] Amanda Howard, Yucheng Fu, and Panos Stinis. A multifidelity approach to continual learning for physical systems. *Machine Learning: Science and Technology*, 5(2):025042, 2024.
- [48] Lu Lu, Raphaël Pestourie, Steven G Johnson, and Giuseppe Romano. Multifidelity deep neural operators for efficient learning of partial differential equations with application to fast inverse design of nanoscale heat transport. *Physical Review Research*, 4(2):023210, 2022.
- [49] Amanda A. Howard, Mauro Perego, George E. Karniadakis, and Panos Stinis. Multifidelity deep operator networks, 2022.
- [50] Subhayan De, Matthew Reynolds, Malik Hassanaly, Ryan N King, and Alireza Doostan. Bi-fidelity modeling of uncertain and partially unknown systems using DeepONets. *Computational Mechanics*, 71(6):1251–1267, 2023.
- [51] Xuhui Meng, Hessam Babaei, and George Em Karniadakis. Multi-fidelity bayesian neural networks: Algorithms and applications. *Journal of Computational Physics*, 438:110361, 2021.
- [52] Mingming Su, Ning Guo, and Zhongxuan Yang. A multifidelity neural network (mfnn) for constitutive modeling of complex soil behaviors. *International Journal for Numerical and Analytical Methods in Geomechanics*, 47(18):3269–3289, 2023.
- [53] Milad Ramezankhani, Amir Nazemi, Apurva Narayan, Heinz Voggenreiter, Mehrtash Harandi, Rudolf Seethaler, and Abbas S Milani. A data-driven multi-fidelity physics-informed learning framework for smart manufacturing: a composites processing case study. In *2022 IEEE 5th International Conference on Industrial Cyber-Physical Systems (ICPS)*, pages 01–07. IEEE, 2022.
- [54] Xinshuai Zhang, Fangfang Xie, Tingwei Ji, Zaoxu Zhu, and Yao Zheng. Multi-fidelity deep neural network surrogate model for aerodynamic shape optimization. *Computer Methods in Applied Mechanics and Engineering*, 373:113485, 2021.
- [55] Lei He, Weiqi Qian, Tun Zhao, and Qing Wang. Multi-fidelity aerodynamic data fusion with a deep neural network modeling method. *Entropy*, 22(9):1022, 2020.
- [56] Mahmudul Islam, Md Shajedul Hoque Thakur, Satyajit Mojumder, and Mohammad Nasim Hasan. Extraction of material properties through multi-fidelity deep learning from molecular dynamics simulation. *Computational Materials Science*, 188:110187, 2021.
- [57] Debanshu S Khamari and Suraj K Behera. A novel multi-fidelity neural network for response prediction using rotor dynamics and model reduction. *Journal of the Brazilian Society of Mechanical Sciences and Engineering*, 45(11):600, 2023.
- [58] Iliia Chiniforooshan Esfahani. A data-driven physics-informed neural network for predicting the viscosity of nanofluids. *AIP Advances*, 13(2), 2023.
- [59] Miad Boodaghidizaji, Monsurul Khan, and Arezoo M Ardekani. Multi-fidelity modeling to predict the rheological properties of a suspension of fibers using neural networks and gaussian processes. *Physics of Fluids*, 34(5), 2022.
- [60] Milad Saadat, William H Hartt V, Norman J Wagner, and Safa Jamali. Data-driven constitutive meta-modeling of nonlinear rheology via multifidelity neural networks. *Journal of Rheology*, 68(5):679–693, 2024.
- [61] Mohammadamin Mahmoudabadbozchelou, Marco Caggioni, Setareh Shahsavari, William H Hartt, George Em Karniadakis, and Safa Jamali. Data-driven physics-informed constitutive metamodeling of complex fluids: A multifidelity neural network (mfnn) framework. *Journal of Rheology*, 65(2):179–198, 2021.
- [62] Farhad Pourkamali-Anaraki. Kolmogorov-arnold networks in low-data regimes: A comparative study with multilayer perceptrons. *arXiv preprint arXiv:2409.10463*, 2024.
- [63] Eleonora Poeta, Flavio Giobergia, Eliana Pastor, Tania Cerquitelli, and Elena Baralis. A benchmarking study of kolmogorov-arnold networks on tabular data. *arXiv preprint arXiv:2406.14529*, 2024.
- [64] Spyros Rigas, Michalis Papachristou, Theofilos Papadopoulos, Fotios Anagnostopoulos, and Georgios Alexandridis. Adaptive training of grid-dependent physics-informed kolmogorov-arnold networks. *arXiv preprint arXiv:2407.17611*, 2024.
- [65] Maziar Raissi, Paris Perdikaris, and George E Karniadakis. Physics-informed neural networks: A deep learning framework for solving forward and inverse problems involving nonlinear partial differential equations. *Journal of Computational Physics*, 378:686–707, 2019.
- [66] Shengze Cai, Zhiping Mao, Zhicheng Wang, Minglang Yin, and George Em Karniadakis. Physics-informed neural networks (pinns) for fluid mechanics: A review. *Acta Mechanica Sinica*, 37(12):1727–1738, 2021.

- [67] Nisal Ranasinghe, Yu Xia, Sachith Seneviratne, and Saman Halgamuge. Ginn-kan: Interpretability pipelining with applications in physics informed neural networks. *arXiv preprint arXiv:2408.14780*, 2024.
- [68] Subhajt Patra, Sonali Panda, Bikram Keshari Parida, Mahima Arya, Kurt Jacobs, Denys I Bondar, and Abhijit Sen. Physics informed kolmogorov-arnold neural networks for dynamical analysis via efficient-kan and wav-kan. *arXiv preprint arXiv:2407.18373*, 2024.
- [69] Hang Shuai and Fangxing Li. Physics-informed kolmogorov-arnold networks for power system dynamics. *arXiv preprint arXiv:2408.06650*, 2024.
- [70] Tianchi Yu, Jingwei Qiu, Jiang Yang, and Ivan Oseledets. Sinc kolmogorov-arnold network and its applications on physics-informed neural networks. *arXiv preprint arXiv:2410.04096*, 2024.
- [71] James Bradbury, Roy Frostig, Peter Hawkins, Matthew James Johnson, Chris Leary, Dougal Maclaurin, George Necula, Adam Paszke, Jake VanderPlas, Skye Wanderman-Milne, and Qiao Zhang. JAX: composable transformations of Python+NumPy programs, 2018.
- [72] Spyros Rigas and Michalis Papachristou. jaxKAN: A JAX-based implementation of Kolmogorov-Arnold Networks, May 2024.
- [73] Chi Chiu SO and Siu Pang YUNG. Higher-order-relu-kans (hrkans) for solving physics-informed neural networks (pinn) more accurately, robustly and faster.
- [74] Han Gao, Luning Sun, and Jian-Xun Wang. Super-resolution and denoising of fluid flow using physics-informed convolutional neural networks without high-resolution labels. *Physics of Fluids*, 33(7), 2021.
- [75] Mykhaylo Zayats, Małgorzata J Zimoń, Kyongmin Yeo, and Sergiy Zhuk. Super resolution for turbulent flows in 2d: stabilized physics informed neural networks. In *2022 IEEE 61st Conference on Decision and Control (CDC)*, pages 3377–3382. IEEE, 2022.
- [76] Kaicheng Yang, Xia Liu, Wenhui Feng, Feng Lian, and Yinan Kong. A super resolution flow field reconstruction method using pinn. In *First Aerospace Frontiers Conference (AFC 2024)*, volume 13218, pages 874–883. SPIE, 2024.
- [77] Shengze Cai, Callum Gray, and George Em Karniadakis. Physics-informed neural networks enhanced particle tracking velocimetry: An example for turbulent jet flow. *IEEE Transactions on Instrumentation and Measurement*, 2024.
- [78] Yongji Wang and Ching-Yao Lai. Multi-stage neural networks: Function approximator of machine precision. *Journal of Computational Physics*, page 112865, 2024.
- [79] Ziad Aldirany, Régis Cottureau, Marc Laforest, and Serge Prudhomme. Multi-level neural networks for accurate solutions of boundary-value problems. *Computer Methods in Applied Mechanics and Engineering*, 419:116666, 2024.
- [80] Mark Ainsworth and Justin Dong. Galerkin neural networks: A framework for approximating variational equations with error control. *SIAM Journal on Scientific Computing*, 43(4):A2474–A2501, 2021.
- [81] Mark Ainsworth and Justin Dong. Galerkin neural network approximation of singularly-perturbed elliptic systems. *Computer Methods in Applied Mechanics and Engineering*, 402:115169, 2022.
- [82] Emma Lejeune. Mechanical mnist - multi-fidelity, 2020.
- [83] Emma Lejeune. Mechanical mnist: A benchmark dataset for mechanical metamodels. *Extreme Mechanics Letters*, 36:100659, 2020.
- [84] Li Deng. The mnist database of handwritten digit images for machine learning research [best of the web]. *IEEE signal processing magazine*, 29(6):141–142, 2012.
- [85] Philipp Holl and Nils Thuerey. Φ_{flow} (PhiFlow): Differentiable simulations for pytorch, tensorflow and jax. In *International Conference on Machine Learning*. PMLR, 2024.
- [86] Seyd Teymoor Seydi. Exploring the potential of polynomial basis functions in kolmogorov-arnold networks: A comparative study of different groups of polynomials. *arXiv preprint arXiv:2406.02583*, 2024.
- [87] Eric AF Reinhardt and Sergei Gleyzer. Sinekan: Kolmogorov-arnold networks using sinusoidal activation functions. *arXiv preprint arXiv:2407.04149*, 2024.
- [88] Hoang-Thang Ta, Duy-Quy Thai, Abu Bakar Siddiqur Rahman, Grigori Sidorov, and Alexander Gelbukh. Fc-kan: Function combinations in kolmogorov-arnold networks. *arXiv preprint arXiv:2409.01763*, 2024.
- [89] Jan Drgona, Aaron Tuor, James Koch, Madelyn Shapiro, and Draguna Vrabie. NeuroMANCER: Neural Modules with Adaptive Nonlinear Constraints and Efficient Regularizations. 2023.

A Training parameters

All results in this paper are implemented in JAX [71] using the Jax-KAN [72] KAN implementation. All networks are trained with the ADAM optimizer.

Boundaries are the iterations at which the grid is refined, following the procedure in [72]. When the grid is refined, the learning rate is scaled using the given scales. If no scales are given, the grid is kept fixed.

A.1 Test 1

| Parameter | |
|----------------------------------|-----------------|
| Low-fidelity KAN architecture | [1, 5, 1] |
| g_L | [5, 10, 15] |
| Low-fidelity scales | [1, .6, .6] |
| Low-fidelity boundaries | [0, 5000, 1000] |
| k_L | 3 |
| Low-fidelity learning rate | 0.001 |
| Low-fidelity iterations | 15001 |
| N_{LF} | 50 and 300 |
| Nonlinear KAN architecture | [2, 4, 1] |
| g_{nl} | 3 |
| k_{nl} | 2 |
| Linear KAN architecture | [2, 1] |
| g_l | 1 |
| k_l | 1 |
| High-fidelity learning rate | 0.005 |
| High-fidelity iterations | 10001 |
| N_{HF} | 5 |
| w | 0 and 10 |
| n | 2 |
| λ_α | 10 |
| Single-fidelity KAN architecture | [1, 2, 1] |
| g | 2 |
| k | 3 |
| Single-fidelity learning rate | 0.005 |
| Single-fidelity iterations | 10001 |

Table 2: Hyperparameters used for the results in section 3.1.

A.2 Test 2

| Parameter | |
|----------------------------------|------------|
| Low-fidelity KAN architecture | [1, 5, 1] |
| g_L | [6, 12] |
| k_L | 3 |
| Low-fidelity learning rate | 0.001 |
| Low-fidelity iterations | 40001 |
| Low-fidelity scales | [1, 0.4] |
| Low-fidelity boundaries | [0, 15000] |
| N_{LF} | 51 |
| Nonlinear KAN architecture | [2, 8, 1] |
| g_{nl} | [5, 8] |
| k_{nl} | 2 |
| Linear KAN architecture | [2, 1] |
| g_l | 1 |
| k_l | 1 |
| High-fidelity learning rate | 0.005 |
| High-fidelity iterations | 100001 |
| High-fidelity scales | [1, 0.7] |
| High-fidelity boundaries | [0, 25000] |
| N_{HF} | 14 |
| w | 0 and 1 |
| n | 4 |
| λ_α | 0.01 |
| Single-fidelity KAN architecture | [1, 5, 1] |
| g | 6 |
| k | 3 |
| Single-fidelity learning rate | 0.001 |
| Single-fidelity iterations | 50001 |

Table 3: Hyperparameters used for the results in section 3.2.

A.3 Test 3

| Parameter | |
|----------------------------------|------------|
| Low-fidelity KAN architecture | [2, 10, 1] |
| g_L | 6 |
| k_L | 3 |
| Low-fidelity learning rate | 0.001 |
| Low-fidelity iterations | 30000 |
| N_{LF} | 10000 |
| Nonlinear KAN architecture | [3, 10, 1] |
| g_{nl} | 5 |
| k_{nl} | 3 |
| Linear KAN architecture | [3, 1] |
| g_l | 1 |
| k_l | 1 |
| High-fidelity learning rate | 0.008 |
| High-fidelity iterations | 50000 |
| N_{HF} | 150 |
| w | 0.001 |
| n | 4 |
| λ_α | 10 |
| Single-fidelity KAN architecture | [2, 10, 1] |
| g | 5 |
| k | 3 |
| Single-fidelity learning rate | 0.008 |
| Single-fidelity iterations | 50000 |

Table 4: Hyperparameters used for the results in section 3.3.

A.4 Test 4

| Parameter | |
|----------------------------------|-------------------|
| Low-fidelity KAN architecture | [4, 10, 1] |
| g_L | [6, 12] |
| k_L | 3 |
| Low-fidelity learning rate | 0.005 |
| Low-fidelity iterations | 15000 |
| Low-fidelity scales | [1, .7] |
| Low-fidelity boundaries | [0, 10000] |
| N_{LF} | 25000 |
| Nonlinear KAN architecture | [5, 6, 1] |
| g_{nl} | 5 |
| k_{nl} | 3 |
| Linear KAN architecture | [5, 1] |
| g_l | 1 |
| k_l | 1 |
| High-fidelity learning rate | 0.008 |
| High-fidelity iterations | 40000 |
| N_{HF} | 150 |
| w | 1 |
| n | 4 |
| λ_α | 10 |
| Single-fidelity KAN architecture | [4, 10, 1] |
| g | [5, 8, 10] |
| k | 3 |
| Single-fidelity learning rate | 0.008 |
| Single-fidelity iterations | 50000 |
| Single-fidelity scales | [1, .8, .8] |
| Single-fidelity boundaries | [0, 20000, 40000] |

Table 5: Hyperparameters used for the results in section 3.4.

A.5 Test 5

| Parameter | |
|----------------------------------|-------------------|
| Low-fidelity KAN architecture | [1, 10, 1] |
| g_L | [6, 12, 18] |
| k_L | 3 |
| Low-fidelity learning rate | 0.0005 |
| Low-fidelity iterations | 60000 |
| Low-fidelity scales | [1, .8, .8] |
| Low-fidelity boundaries | [0, 20000, 40000] |
| N_{LF} | 1000 |
| Nonlinear KAN architecture | [2, 10, 10, 1] |
| g_{nl} | [6, 12, 18] |
| k_{nl} | 3 |
| Linear KAN architecture | [2, 1] |
| g_l | 1 |
| k_l | 1 |
| High-fidelity learning rate | 0.01 |
| High-fidelity iterations | 60000 |
| High-fidelity scales | [1, .8, .8] |
| High-fidelity boundaries | [0, 20000, 40000] |
| N_{HF} | 1000 |
| w | 0 |
| n | 4 |
| λ_α | 100000 |
| Single-fidelity KAN architecture | [1, 8, 8, 1] |
| g | [6, 12, 18] |
| k | 3 |
| Single-fidelity learning rate | 0.0005 |
| Single-fidelity iterations | 60000 |
| Single-fidelity scales | [1, .8, .8] |
| Single-fidelity boundaries | [0, 20000, 40000] |

Table 6: Hyperparameters used for the results in section 3.5.

A.6 Test 6

| Parameter | |
|----------------------------------|--------------|
| Low-fidelity KAN architecture | [784, 64, 1] |
| g_L | 5 |
| k_L | 3 |
| Low-fidelity learning rate | 0.01 |
| Low-fidelity iterations | 30001 |
| N_{LF} | 60000 |
| Nonlinear KAN architecture | [785, 32, 1] |
| g_{nl} | 5 |
| k_{nl} | 3 |
| Linear KAN architecture | [1, 1] |
| g_l | 1 |
| k_l | 1 |
| High-fidelity learning rate | 0.01 |
| High-fidelity iterations | 60001 |
| w | 0 |
| n | 4 |
| λ_α | 0.01 |
| Single-fidelity KAN architecture | [784, 64, 1] |
| g | 5 |
| k | 3 |
| Single-fidelity learning rate | 0.01 |
| Single-fidelity iterations | 60001 |

Table 7: Hyperparameters used for the results in section 3.6.

A.7 Test 7

| Parameter | |
|----------------------------------|---|
| Nonlinear KAN architecture | [3, 40, 40, 1] |
| g_{nl} | [5, 10, 15] |
| k_{nl} | 3 |
| Linear KAN architecture | [3, 1] |
| g_l | 1 |
| k_l | 1 |
| High-fidelity learning rate | 0.005 |
| High-fidelity iterations | 100000 |
| High-fidelity scales | [1, .8, .8] |
| High-fidelity boundaries | [0, 20000, 40000] |
| N_{HF} | 100 time snapshots, 33153 points per snapshot |
| w | 0 |
| n | 4 |
| λ_α | 0.01 |
| Single-fidelity KAN architecture | [3, 40, 40, 1] |
| g | [5, 10, 15] |
| k | 3 |
| Single-fidelity learning rate | 0.01 |
| Single-fidelity iterations | 100000 |
| Single-fidelity scales | [1, .8, .8] |
| Single-fidelity boundaries | [0, 20000, 40000] |

Table 8: Hyperparameters used for the results in section 3.7.